JOURNAL OF MATERIALS SCIENCE **40** (2005) 6463–6472

Self-sensing of damage in carbon fiber polymer-matrix composite by measurement of the electrical resistance or potential away from the damaged region

SHOUKAI WANG, D. D. L. CHUNG*
Composite Materials Research Laboratory, University at Buffalo, State University of New York, Buffalo, NY 14260-4400, USA
E-mail: ddlchung@buffalo.edu

JAYCEE H. CHUNG
Global Contour Ltd., 1145 Ridge Road West, Rockwall, TX 75087

Published online: 5 October 2005

Self-sensing of damage by measurement of the DC electrical resistance or potential away from the damaged region was demonstrated in quasi-isotropic continuous carbon fiber epoxy-matrix composite laminates under impact at energy up to 5 J. The through-thickness potential was substantial up to 240– 480 mm (at 0.25–99 mA correspondingly) in the longitudinal direction from the position of through-thickness current application, due to current spreading in the longitudinal direction. A model for the current spreading is provided. The fractional change in resistance resulting from damage decreased with increasing distance from the point of impact (diameter of indentation up to 3.5 mm and depth of indentation up to 0.16 mm), such that it was non-zero even at a distance of 150 mm from the point of impact. Both the through-thickness resistance and the oblique resistance were effective indicators. The ability for the resistance measured away from the damaged region to indicate damage in the damaged region is due to the much lower electrical resistivity in the longitudinal than through-thickness or oblique directions in the composite.

1. Introduction

A structure may suffer from damage due to live loads, abuse, accidents, aging, mechanical fatigue, corrosion, thermal stress, lightning and various environmental factors. For the purpose of hazard mitigation, it is important to monitor the damage. Detection of damage allows repair, replacement or operation adjustment. Real-time monitoring, as opposed to occasional monitoring, is particularly attractive, as it allows damage to be detected as soon as it is inflicted.

Damage monitoring, also known as structural health monitoring, involves the use of damage sensors. A conventional method involves the embedment of sensors (such as fiber optic sensors [1, 2]) in a structure. A related conventional method involves the attachment of sensors (such as piezoelectric sensors [3–5]) on a structure. These conventional methods suffer from their poor durability and high cost compared to structural materials. In the case of embedded sensors, further disadvantages pertain to the loss in mechanical properties and the difficulty of repairing the sensors.

An unconventional method of damage monitoring involves the use of the structural material itself as the sensor, so that there is no embedded or attached sensor. The structural material is low cost and durable. A structure made with a self-sensing structural material has its entire volume capable of sensing, in contrast to the limited sensing volume in the case of embedded or attached sensors. As a consequence, the problems associated with embedded or attached sensors, as mentioned above, are greatly alleviated. This unconventional method is known as self-sensing.

Polymer-matrix composites containing continuous carbon fiber reinforcement are dominant among lightweight structural composites. This is due to their high strength, high modulus and low density. They are widely used for aircraft structures [6–8]. Due to the aging and safety requirement of aircraft, damage monitoring is critically needed for both military and civil aircraft.

Self-sensing has been shown in carbon fiber polymer-matrix composites, as made possible by DC

*Author to whom all correspondence should be addressed.
0022-2461
DOI: 10.1007/s10853-005-1708-2

electrical resistance [9–27] or potential [28, 29] measurement. Due to the electrical conductivity of carbon fibers, the composite is conductive and damage can affect the electrical resistivity of the composite. Damage in the form of delamination increases the resistivity in the direction perpendicular to the fiber layers [30]. Damage in the form of fiber breakage increases the resistivity in the direction of the fibers [31].

Damage sensing is to be distinguished from strain sensing [32–34], which refers to the sensing of reversible strain in the absence of damage. Strain sensing is useful for structural vibration control and weighing.

In spite of the advances made in the area of damage self-sensing in carbon fiber polymer-matrix composites, spatially resolving damage self-sensing has not been previously reported. As a practical structural component tends to be large, the damage in it is usually localized. The determination of the location of the damage is necessary for the purpose of repair. Spatially resolved sensing would allow determination of the damage location, in addition to determining the damage distribution.

This paper is aimed at investigating the ability of carbon fiber epoxy-matrix composite for the self-sensing of damage by measurement of the electrical resistance or potential away from the damaged region. The allowed distance between the measurement position and the damage position is relevant to practical implementation of the damage self-sensing technology. This aim is also related to spatially resolved self-sensing, as a larger allowed distance means less spatial resolution. For this purpose, the DC electrical resistance or potential is measured in different locations of a composite specimen with or without damage. In this work, the damage is local, as inflicted by drop impact. In addition, the resistance or potential is measured in various directions of the composite for the purpose of investigating the relative effectiveness of resistances in various directions for damage sensing. These directions include the through-thickness direction and an oblique direction (a direction between the longitudinal direction and the through-thickness direction of the laminate).

2. Experimental methods

Commercially manufactured composites in the form of continuous carbon fiber (Hercules IM6, a high-performance intermediate-modulus, PAN-based fiber in the form of 12000 filament count tows) epoxy-matrix (Hercules 3501-6, cured at 177°C) laminates of fiber volume fraction 63.5% were cut into strips of length 200 mm (or more) in the 0° direction and width either 10 or 12 mm in the 90° direction and then sanded by using 600 grit silicon carbide sand paper for the purpose of removing the surface layer (about 20 μm

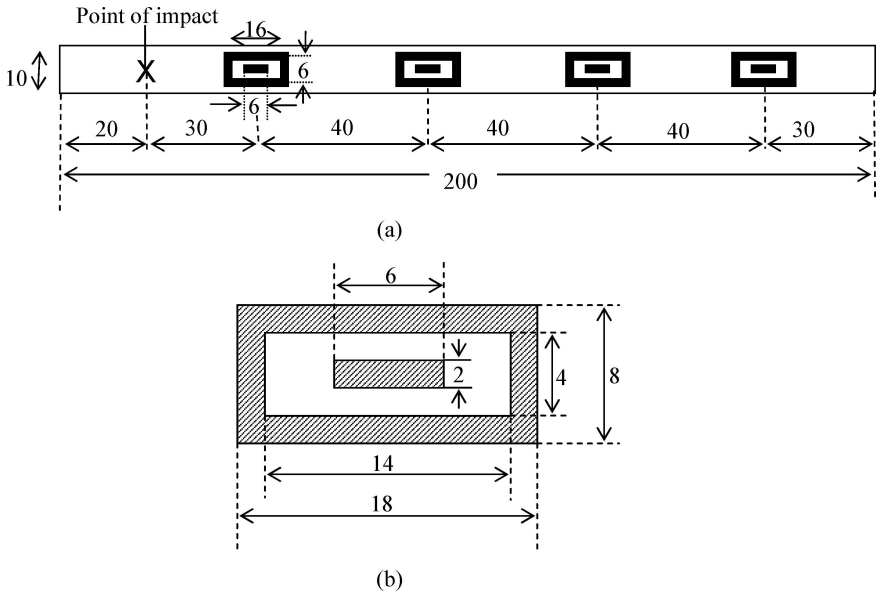

Figure 1 Specimen configuration for measuring the through-thickness resistance at various distances from the point of impact. All dimensions are in mm. (a) Top view of the entire specimen. (b) A detailed view of a set of current and voltage contacts.

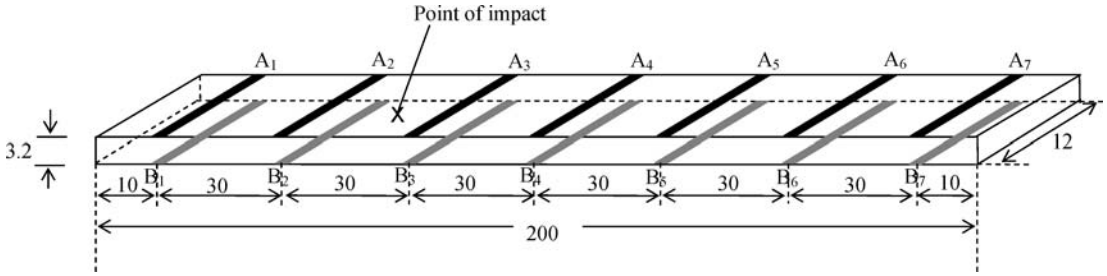

Figure 2 Specimen configuration for measuring the oblique resistance at various distances from the point of impact. All dimensions are in mm. The width of each electrical contact is 2 mm.

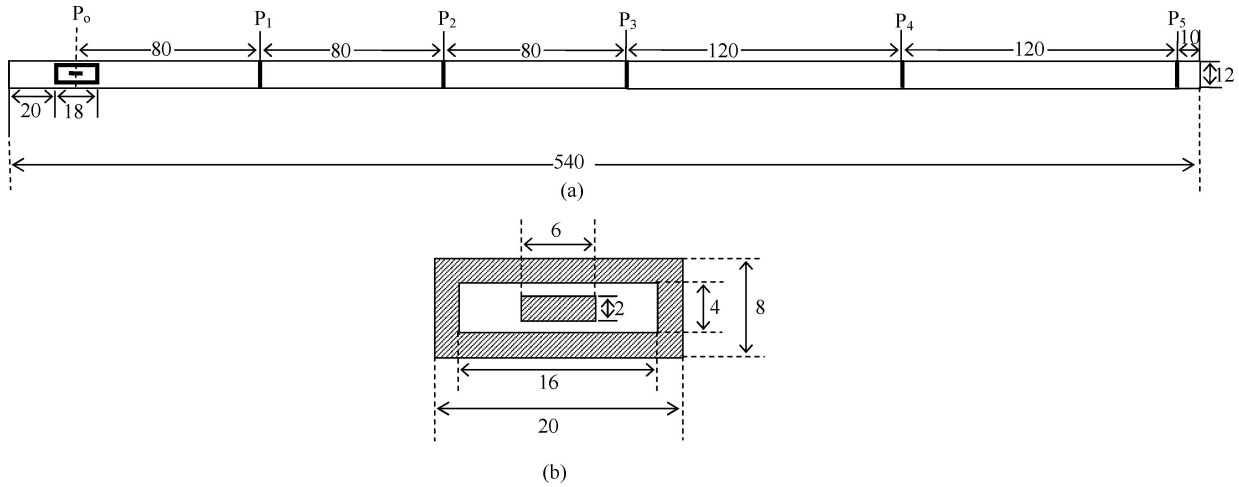

Figure 3 Specimen configuration for measuring the though-thickness potential at various distances from the point of impact. All dimensions are in mm. (a) Top view of the entire specimen. (b) A detailed view of the current contact and a voltage contact, both at P_o.

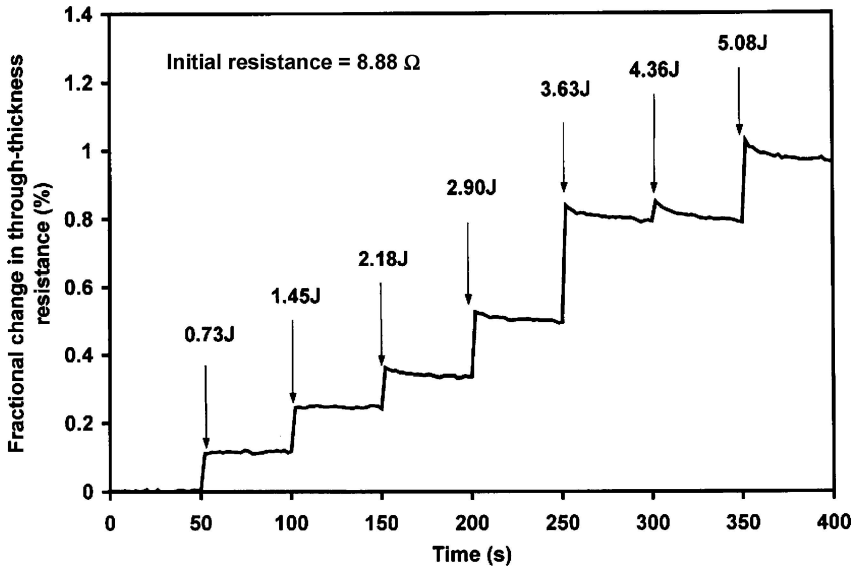

Figure 4 Fractional change in through-thickness resistance vs. time at progressively increasing impact energy at a fixed distance of 30 mm from the point of impact. The specimen is the 24-lamina quasi-isotropic composite.

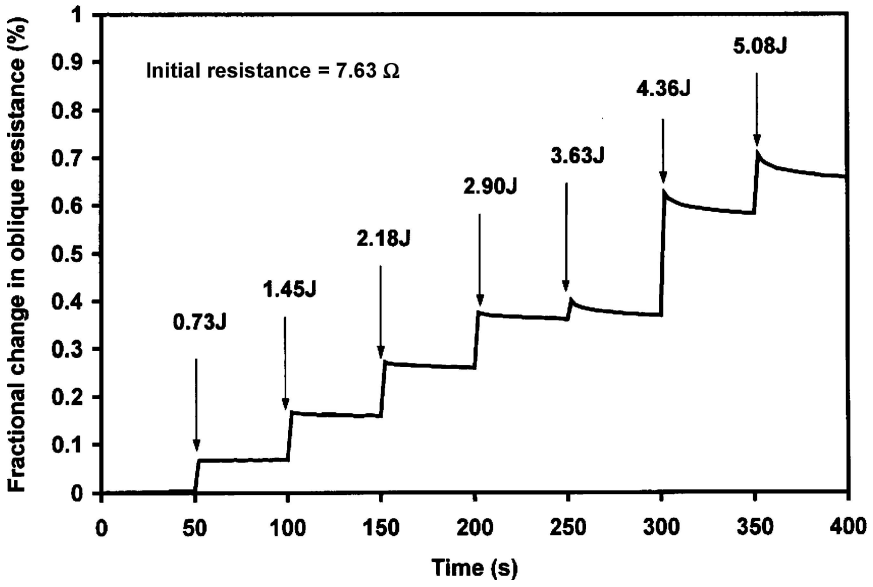

Figure 5 Fractional change in oblique resistance vs. time at progressively increasing impact energy at a distance of 0 mm from the point of impact. The specimen is the 24-lamina quasi-isotropic composite.

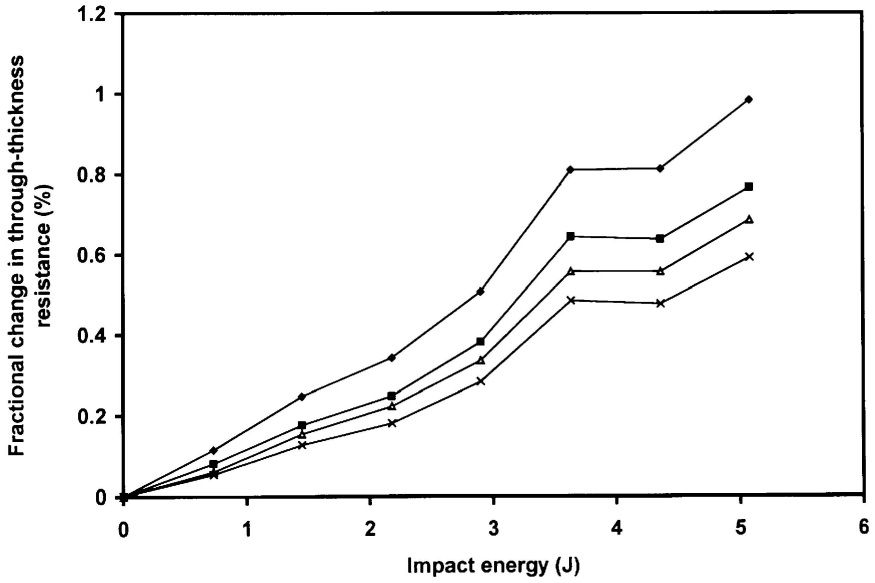

Figure 6 Fractional change in through-thickness resistance vs. impact energy. The specimen is the 24-lamina quasi-isotropic composite: (♦), 30 mm from point of impact (initial resistance = 8.88 Ω); (■), 70 mm from point of impact (initial resistance = 9.67 Ω); (Δ), 110 mm from point of impact (initial resistance = 9.84 Ω); (×), 150 mm from point of impact (initial resistance = 10.63 Ω).

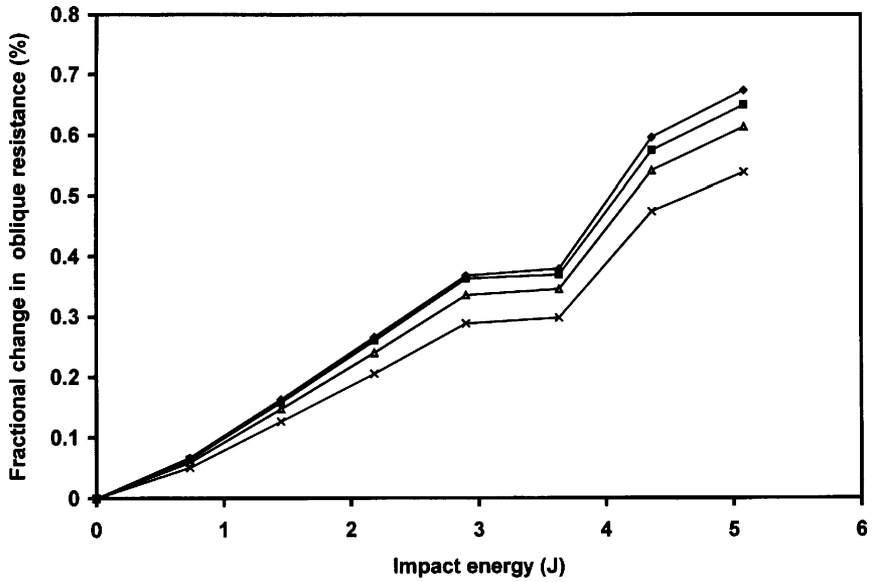

Figure 7 Fractional change in oblique resistance vs. impact energy. The specimen is the 24-lamina quasi-isotropic composite: (♦), 0 mm from point of impact (initial resistance = 7.63 Ω); (■), 30 mm from point of impact (initial resistance = 7.44 Ω); (Δ), 60 mm from point of impact (initial resistance = 7.46 Ω); (×), 90 mm from point of impact (initial resistance = 7.89 Ω).

thick) of epoxy matrix prior to the application of electrical contacts. The contacts were in the form of silver paint in conjunction with copper wire. After application, each contact was protected by an epoxy coating, which helped to avoid mechanical degradation of the contact. The sanding step is not essential, but it helps the electrical measurement by increasing the accuracy and decreasing the noise. Although the entire surface was sanded in this work, only the portions beneath the electrical contacts needed to be sanded.

Unless noted otherwise, the laminate had 24 laminae in the quasi-isotropic $[0/45/90/-45]_{3s}$ lay-up configuration. The thickness was 3.2 mm.

DC electrical resistance or potential measurement was conducted using the four-probe method. In this method, the outer two electrical contacts are for passing current, while the inner two electrical contacts are for voltage measurement. In this way, the measured resistance of the part of the specimen between the voltage contacts does not include the resistance of the two voltage contacts. In contrast, the two-probe method involves two rather than four electrical contacts, and consequently the measured resistance includes the

TABLE I Depth of indentation at various impact energies

Impact energy (J)	Diameter[a] (mm)	Depth[b] (mm)
0.73	1.0	0.013
1.45	1.1	0.016
2.18	2.1	0.058
2.90	3.2	0.14
3.63	3.4	0.15
4.36	3.5	0.16
5.08	3.5	0.16

[a]Measured.
[b]Calculated from the measured diameter.

TABLE II Through-thickness potential at various distances from P_o (P_o defined in Fig. 3)

	Potential (mV)						
Distance from P_o (mm)	0.25 mA	4.17 mA	9.19 mA	19.2 mA	29.2 mA	49.1 mA	99.3 mA
0	2.636	13.184	26.367	52.722	79.102	131.808	263.464
80	0.530	2.657	5.317	10.633	15.953	26.586	53.152
160	0.157	0.800	1.605	3.212	4.820	8.034	16.066
240	0.055	0.276	0.552	1.105	1.658	2.763	5.524
360	0.008	0.042	0.086	0.173	0.260	0.433	0.867
480	0.000	0.006	0.012	0.025	0.038	0.064	0.128

TABLE III Through thickness potential relative to the value at P_o at various distances from P_o (P_o defined in Fig. 3)

	Potential relative to value at P_o (%)						
Distance from P_o (mm)	0.25 mA	4.17 mA	9.19 mA	19.2 mA	29.2 mA	49.1 mA	99.3 mA
0	100	100	100	100	100	100	100
80	20.10	20.15	20.16	20.17	20.17	20.17	20.17
160	5.96	6.07	6.09	6.09	6.09	6.10	6.10
240	2.07	2.09	2.09	2.10	2.10	2.10	2.10
360	0.29	0.32	0.33	0.33	0.33	0.33	0.33
480	0.02	0.04	0.05	0.05	0.05	0.05	0.05

resistance of the two contacts. A Keithley 2002 multimeter was used.

For through-thickness resistance measurement, the specimen was 200 mm long and 10 mm wide, with four sets of electrical contacts on the top surface (the surface at which drop impact was directed) and four other sets on the bottom surface, such that the sets on the two surfaces were directly opposite one another (Fig. 1a). Each set of electrical contacts was in the form of a rectangular loop, which served as the current contact, and a strip inside to loop to serve as the voltage contact. Fig. 1b shows a detailed view of a set of contacts. The point of impact was on the top surface (surface shown in Fig. 1a) at a distance of 20 mm from one end of the specimen.

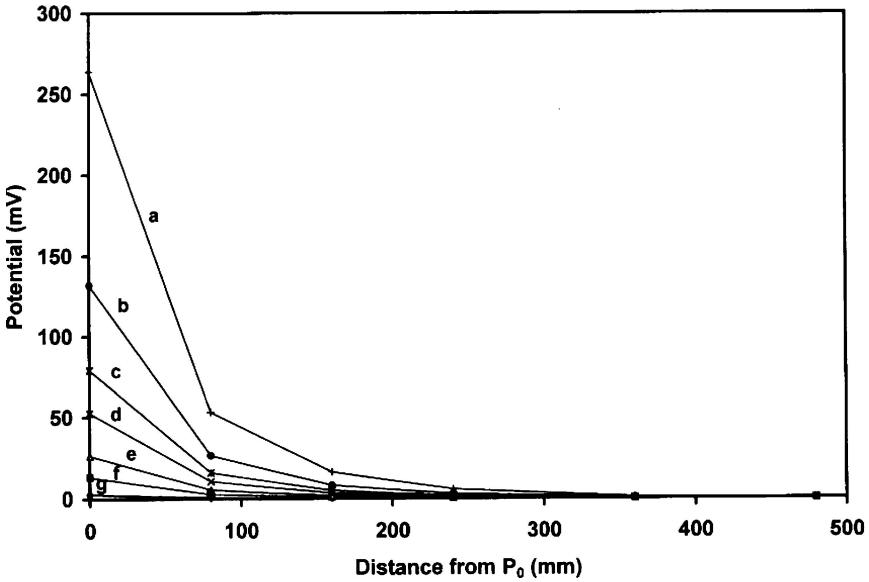

Figure 8 Variation of the through-thickness potential with the distance from P_o (P_o defined in Fig. 3) in the longitudinal direction in the absence of damage. (a) 99.3 mA, (b) 49.1 mA, (c) 29.2 mA, (d) 19.2 mA, (e) 9.19 mA, (f) 4.17 mA, (g) 0.25 mA. The specimen is the 8-lamina quasi-isotropic composite.

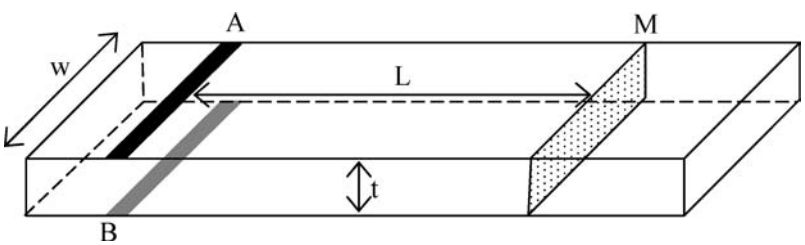

Figure 9 Configuration for calculating the extent of current spreading in the longitudinal direction. *A* and *B* are current contacts for through-thickness resistance measurement. *M* is a plane at a distance of *d* from the plane containing *A* and *B*.

The four sets of electrical contacts on the top surface were centered at points that were at distances of 30, 70, 110 and 150 mm from the point of impact. The four sets of contacts on the bottom surface were similarly located, such that the two sets that were directly opposite one another constituted four electrical contacts, as needed for the four-probe method. Thus, the through-thickness resistances at the four locations relative to the point of impact were simultaneously measured as the impact energy was progressively increased. The impact was repeatedly directed at the same point while the impact energy increased step by step (time period of 50 s per step). The through-thickness resistance was not measured at the point of impact.

For oblique resistance measurement, the specimen was 200 mm long and 12 mm wide, with seven electrical contacts in the form of parallel strips on the top surface (labeled $A_1, A_2, \ldots, A_7$ in Fig. 2) and seven other contacts on the bottom surface (labeled $B_1, B_2, \ldots, B_7$ in Fig. 2), such that the contacts on the two surfaces were directly opposite. The point of impact was between A_2 and A_3 on the top surface. The oblique resistance at the point of impact was measured by using A_1 and B_4 as current contacts and A_2 and B_3 as voltage contacts. The oblique resistance at a distance of 30 mm from the point of impact was measured by using A_2 and B_5 as current contacts and A_3 and B_4 as voltage contacts. The oblique resistance at a distance of 60 mm from the point of impact was measured by using A_3 and B_6 as current contacts and A_4 and B_5 as voltage contacts. The oblique resistance at a distance of 90 mm from the point of impact was measured by using A_4 and B_7 as current contacts and A_5 and B_6 as voltage contacts. The degree of obliqueness was the same for each distance from the point of impact. The oblique resistance at distances of 0, 30, 60 and 90 mm from the point of impact were successively measured at times that were less than 0.3 s from one another while the impact energy increased step by step (time period of 50 s per step). The impact was repeatedly directed at the same point.

For through-thickness potential measurement, an 8-lamina quasi-isotropic $[0/45/90/-45]_s$ composite of thickness 1.0 mm was used. The specimen was 540 mm long (in the 0° direction) and 12 mm wide, with two identical sets of electrical contacts on the top and bottom surfaces. The contacts P_1, P_2, P_3, P_4 and P_5 were for potential measurements at five positions and were in the form of strips in the transverse directions (Fig. 3a). The contacts P_o were in the form of a rectangular loop, which served as the current contact, and a strip inside the loop to serve as the voltage contacts (Fig. 3b). Thus, the current contacts were fixed at P_o, while various sets of voltage contacts (at P_o, P_1,. . .P_5) were used for potential measurement.

The damage resulted in an indentation, the diameter of which was measured by using calipers in order to provide a rough indication of the extent of damage. The depth of the indentation was calculated from the diameter of the indentation and the diameter of the impacting hemisphere. Each indentation was made with a single impact at a selected impact energy, in contrast to the multiple impacts made at the same point at successively increasing energies for the electrical resistance monitoring. The damaged area was probably larger than the indented area.

3. Results and discussion

3.1. Resistance measurement

Both the through-thickness resistance (Fig. 4) and the oblique resistance (Fig. 5) increased irreversibly and abruptly at each impact. The higher the impact energy,

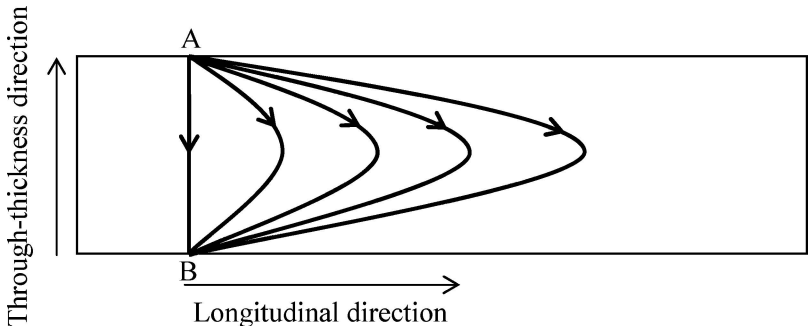

Figure 10 Multiple through-thickness current paths due to current spreading in the longitudinal direction. *A* and *B* correspond to those in Fig. 9.

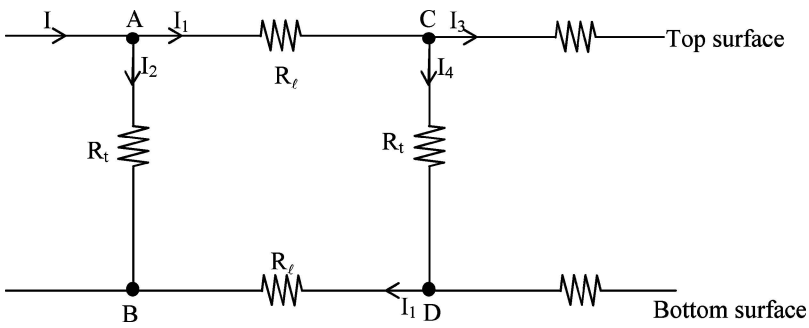

Figure 11 Electric circuit model for multiple current paths.

the greater was the resistance after impact. As the impacts at increasing energy were directed at the same point, the resistance in any position reflected the cumulative damage at the point of impact.

Fig. 6 shows the fractional change in through-thickness resistance vs. impact energy for distances of 30, 70, 110 and 150 mm from the point of impact. For any of the distances, the resistance increased monotonically with increasing impact energy. For any of the impact energies, the resistance decreased monotonically with increasing distance from the point of impact.

Fig. 7 shows the fractional change in oblique resistance vs. impact energy for distances of 0, 30, 60 and 90 mm from the point of impact. For any of the distances, the resistance increased monotonically with increasing impact energy. For any of the impact energies, the resistance decreased monotonically with increasing distance from the point of impact.

Comparison of Figs 6 and 7 shows that the resistance decreases with distance from the point of impact more significantly for the through-thickness resistance than the oblique resistance. Moreover, the oblique resistance allows measurement of the resistance at the point of impact, whereas the through-thickness resistance does not. Furthermore, the electrical contact scheme is simpler for the oblique resistance. Thus, the oblique resistance is more attractive than the through-thickness resistance for indicating damage, particularly damage that is at a distance from where the resistance is measured.

Although Figs 6 and 7 were both for the 24-lamina composite, they were not obtained on the same piece of specimen. The difference in specimen is responsible for the impact energy of 3.63 J causing essentially no change in through-thickness resistance in Fig. 6, but causing a relatively sharp increase in oblique resistance in Fig. 7.

The severity of damage at the point of impact is indicated by the fractional change in resistance (through-thickness or oblique) at a position that can be away from the damaged region. The degree of indication (i.e., the

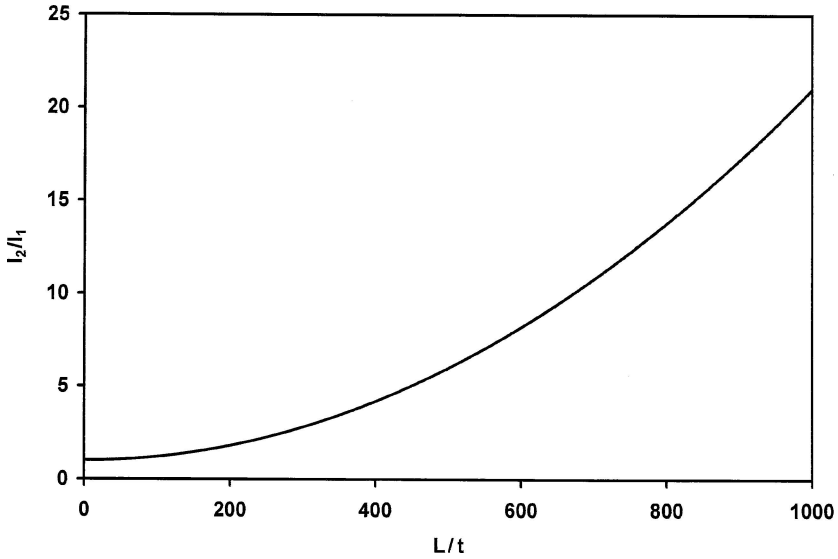

Figure 12 Plot of I_2/I_1 vs. L/t, using Equation 10.

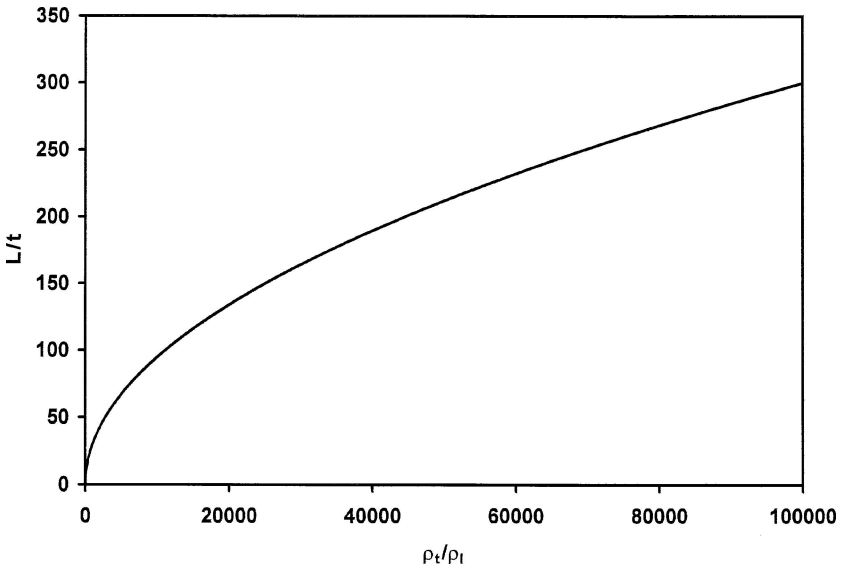

Figure 13 Relationship of L/t and ρ_t/ρ_ℓ for the case of $I_2/I_1 = 2.8$.

fractional change in resistance) diminishes as the distance from the point of impact increases, but the degree of indication is non-zero even at a distance of 150 mm from the point of impact, irrespective of the severity of the damage at the point of impact. This means that it is possible to sense damage by measuring the resistance away from the damaged region.

The through-thickness resistance, whether before and after impact, was higher than the oblique resistance. This is due to the high through-thickness resistivity compared to the longitudinal resistivity. In spite of the short current path for through-thickness resistance measurement compared to the path for oblique resistance measurement, the through-thickness resistance was higher than the oblique resistance.

Due to the relatively low longitudinal resistivity, the through-thickness current path spreads in the longitudinal direction. Due to the spreading, the resistance at a point away from the damaged region cannot indicate the relatively minor damage, if any, at this same point. Nevertheless, it reflects the relatively major damage in the damaged region. Current spreading affects the through-thickness resistance more than the oblique resistance. This is due to the relatively large distance between the voltage contacts used for measuring the oblique resistance.

The Appendix provides a model of through-thickness current spreading in the longitudinal direction. This model shows that the extent of current spreading can be much more than 150 mm. As a consequence, the increase in the measured through-thickness resistance at a distance of 150 mm from the point of impact is dominated by the damage at the point of impact, whether or not minor damage exists at a distance of 150 mm from the point of impact.

The oblique resistance is expected to be more sensitive to fiber fracture than the through-thickness resistance. That the fractional change in through-thickness resistance is higher than that in oblique resistance for the same impact energy means that the damage was predominantly delamination rather than fiber fracture. The dominance of delamination over fiber fracture is typical in carbon fiber polymer-matrix composites, unless the damage is so severe that failure is approached.

Table I shows the depth of indentation at various impact energies. In the regime of low impact energy (less than 1.5 J), the depth of indentation is so small that the indentation is almost invisible to the naked eyes. Even at the highest impact energy of 5.08 J, the depth of indentation is small compared to the thickness of the composite. Delamination was not observed visually, but likely occurred in a microscopic scale.

3.2. Potential measurement

Table II shows the variation of the through-thickness potential with the distance from P_o in the longitudinal direction (P_o defined in Fig. 3) in the absence of damage. Table III shows the same results in terms of the potential relative to the value at P_o. The potential decreased with increasing distance, such that the incremental decrease became less significant as the distance increased. The greater was the current used, the higher was the potential (as expected), but the slightly more was the fractional decrease in potential at the same distance.

In practical self-sensing, the allowed distance between the potential measurement position and the current application position is the maximum distance for the measured potential to be substantial (at least 0.1 mV), i.e., the maximum distance for sensing. The higher was the current, the larger was this distance. This distance in the longitudinal direction was 160, 240, 240, 360, 360, 360 and 480 mm at a current of 0.25, 4.17, 9.19, 19.2, 29.2, 49.1 and 99.3 mA respectively. This distance relates to that for which the current (applied in the through-thickness direction) traveled in the longitudinal direction. Due to the relatively low resistivity in the longitudinal direction, the current traveled up to 480 mm in the longitudinal direction. This extent of travel is consistent with the model of current spreading in the Appendix. For directions other than the longitudinal direction, the resistivity is expected to be higher and thus the distance of current travel is expected to be smaller. In order for the spatial resolution in damage self-sensing to be better than this distance, the functional relationship (Fig. 8) between the measured potential and the distance (between the potential measurement position and the current application position) needs to be considered, in addition to considering the value of the potential.

4. Conclusion

Damage self-sensing by electrical resistance or potential measurement away from the damaged region was demonstrated in carbon fiber epoxy-matrix composite laminates. The damage was inflicted by drop impact at energy from 0.7 to 5 J. The through-thickness potential was substantial up to 240 mm at a current of 0.25 mA and up to 480 mm at a current of 99 mA, in the longitudinal direction from the position of through-thickness current application. This is due to current spreading in the longitudinal direction. A model for the current spreading is provided. The fractional change in resistance resulting from the damage decreased with increasing distance from the point of impact, such that it was non-zero even at a distance of 150 mm from the point of impact. The indentation resulted from the impact was up to 3.5 mm in diameter (compared to a damage zone of radius at least 150 mm) and up to 0.16 mm in depth (compared to a specimen thickness of 3.2 mm). The resistance was either the through-thickness resistance or the oblique resistance. The response to damage was similar for these two resistances, but the through-thickness resistance dropped with distance from the point of impact more significantly than the oblique resistance. The electrical contact scheme was simpler for the oblique resistance.

Appendix

This appendix provides a model of through-thickness current spreading in the longitudinal direction.

Consider a configuration in which the current contacts A and B are in the form of strips on opposite sides of a composite bar (Fig. 9). This configuration is relevant to the measurement of the through-thickness resistance. The question pertains to the distance L of longitudinal spreading of the current that is applied in the through-thickness direction between A and B. Consider the segment of the specimen between the AB plane and the M plane in Fig. 7. If the longitudinal resistance is much smaller than the through-thickness resistance of this segment, the distance of current spreading in the longitudinal direction will be large. Thus, the current spreading depends on the relative values of these resistances.

In reality, there is a continum of paths of current flow resulting from the current spreading, as illustrated in Fig. 10. The circuit model of multiple paths is shown in Fig. 11, where R_t is the through-thickness resistance of an element of width $\ell/2$ in the longitudinal direction and length t in the through-thickness direction, and R_ℓ is the longitudinal resistance of an element of length ℓ in the longitudinal direction and width $t/2$ in the through-thickness direction. With w being the specimen dimension perpendicular to the page in Fig. 10,

$$R_t = \rho_t \frac{t}{w\ell/2} \tag{1}$$

and

$$R_\ell = \rho_\ell \frac{\ell}{wt/2}, \tag{2}$$

where ρ_t is the through-thickness resistivity and ρ_ℓ is the longitudinal resistivity.

When $\ell = L$ (where L is the extent of current spreading), $I_3 = 0$ in Fig. 11. Under this situation,

$$I_4 = I_1 - I_3 = I_1 \tag{3}$$

Note that

$$V_{AB} = V_{AC} + V_{CD} + V_{DB}, \tag{4}$$

where V_{AB} is the voltage difference between A and B, V_{AC} is the voltage difference between A and C, V_{CD} is the voltage difference between C and D, and V_{DB} is the voltage difference between D and B. Equation 4 can be written as

$$I_2 R_t = I_1 R_\ell + I_4 R_t + I_1 R_\ell \tag{5}$$

Using Equation 3, Equation 5 becomes

$$I_2 R_t = I_1 (2R_\ell + R_t) \tag{6}$$

Rearrangement of Equation 6 gives

$$\frac{I_2}{I_1} = \frac{2R_\ell + R_t}{R_t} = \frac{2R_\ell}{R_t} + 1 \tag{7}$$

Combination of Equation 7, 1 and 2 gives

$$\frac{I_2}{I_1} = 2\frac{\rho_\ell}{\rho_t}\left(\frac{L}{t}\right)^2 + 1 \tag{8}$$

For the quasi-isotropic composite of thickness 3.2 mm in this work, separate measurements using the four-probe method and silver paint electrical contacts show that $\rho_L = 7$ mΩ·cm and $\rho_T = 600$ Ω·cm. (The specimen size was 22 × 10 × 3.2 mm for ρ_T measurement.) Hence,

$$\rho_T / \rho_L = 10^5 \tag{9}$$

Using Equation 9, Equation 8 becomes

$$\frac{I_2}{I_1} = 2 \times 10^{-5}\left(\frac{L}{t}\right)^2 + 1 \tag{10}$$

Fig. 12 is a plot of Equation 10. The experimental result in Fig. 8 shows that L is approximately 300 mm. Since $t = 1$ mm for the specimen of Fig. 8, $L/t = 300$. Based on Equation 10 or Fig. 12, this value of L/t corresponds to $I_2/I_1 = 2.8$.

For a given value of I_2/I_1, Equation 8 shows that the smaller is ρ_ℓ/ρ_t, the greater is L/t. In other words, a smaller value of ρ_ℓ/ρ_t results in more current spreading, as expected. The lay-up configuration affects ρ_ℓ/ρ_t, thereby affecting the extent of current spreading. Fig. 13 gives the relationship between L/t and ρ_t/ρ_ℓ for the case of $I_2/I_1 = 2.8$.

Acknowledgment

This work was supported in part by the U.S. National Science Foundation.

References

1. D. LIANG, *Electron. Lett.* **29**(6) (1993) 529.
2. K. S. C. KUANG, R. KENNY, M. P. WHELAN, W. J. CANTWELL and P. R. CHALKER, *Smart Mater. Struct.* **10**(2) (2001) 338.
3. M. PORFILIO, *Adv. Space Res.* **34**(5) (2004) 929.
4. S. IMAI, M. TOKUYAMA, S. HIROSE, G. J. BURGER, T. S. J. LAMMERINK and J. H. J. FLUITMAN, *IEEE T. Magn.* **31**(6 pt 1) (1995) 3009.
5. J. HAYWOOD, P. T. COVERLEY, W. J. STASZEWSKI and K. WORDEN, *Smart Mater. Struct.* **14**(1) (2005) 265.
6. A. H. TULLO, *Chem. Eng. News* **82**(35) (2004) 40.
7. O. BARTON JR. and P. H. MILLER, in *ASEE Annual Conference and Exposition: Staying in Tune with Engineering Education*, p. 3321.
8. A. YAHATA and H. KIKUKAWA, R&D Program for Innovative Civil Aircraft Structures. Technical Paper—Society of Manufacturing Engineers ICCM-14 (2004) p. 193.
9. X. WANG and D. D. L. CHUNG, *Smart Mater. Struct.* **6** (1997) 504.
10. X. WANG, F. FU and D. D. L. CHUNG, *J. Mater. Res.* **13**(11) (1998) 3081.
11. X. WANG, S. WANG and D. D. L. CHUNG, *J. Mater. Sci.* **34**(11) (1999) 2703.
12. S. WANG and D. D. L. CHUNG, *Polym. & Polym. Compos.* **9**(2) (2001) 135.
13. *Idem. Comp. Interf.* **9**(1) (2002) 51.
14. S. WANG, Z. MEI and D. D. L. CHUNG, *Int. J. Adh. Adh.* **21**(ER6) (2001) 465.

15. Z. MEI, V. H. GUERRERO, D. P. KOWALIK and D. D. L. CHUNG, *Polym. Compos.* **23**(3) (2002) 425.
16. D. D. L. CHUNG and S. WANG, *Polym. & Polym. Compos.* **11**(7) (2003) 515.
17. K. YOSHITAKE, K. SHIBA, M. SUZUKI, M. SUGITA and Y. OKUHARA, "Damage Evaluation for Concrete Structures using Fiber Reinforced Composites as Self-Diagnosis Materials". Smart Structures and Materials 2004: Smart Sensor Technology and Measurement Systems, Ed. Eric Udd, Daniele Inaudi, Proceedings of SPIE Vol. 5384, (SPIE, Bellingham, WA, 2004), p. 89.
18. M. KUPKE, K. SCHULTE and R. SCHÜLER, *Compos. Sci. Tech.* **61** (2001) 837.
19. K. SCHULTE, *J. De Physique IV, Colloque C7* **3** (1993) 1629.
20. K. SCHULTE and Ch. BARON, *Comp. Sci. Tech.* **36** (1989) 63.
21. A. S. KADDOUR, F. A. R. AL-SALEHI, S. T. S. AL-HASSANI and M. J. HINTON, *ibid.* **51**(3) (1994) 377.
22. O. CEYSSON, M. SALVIA and L. VINCENT, *Scripta Materialia* **34**(8) (1996) 1273.
23. N. MUTO, H. YANAGIDA, M. MIYAYAMA, T. NAKATSUJI, M. SUGITA and Y. OHTSUKA, *J. Ceram. Soc. Jpn, Int. Ed.* **100**(4) (1992) 585.
24. N. MUTO, H. YANAGIDA, T. NAKATSUJI, M. SUGITA, Y. OHTSUKA, Y. ARAI and C. SAITO, *Adv. Compos. Mater.* **4**(4) (1995) 297.
25. N. MUTO, H. YANAGIDA, T. NAKATSUJI, M. SUGITA, Y. OHTSUKA and Y. ARAI, *Smart Mater. Struct.* **1** (1992) 324.
26. J. C. ABRY, S. BOCHARD, A. CHATEAUMINOIS, M. SALVIA and G. GIRAUD, *Compos. Sci. Tech.* **59** (1999) 925.
27. R. PRABHAKARAN, *Experim. Techn.* **14**(1) (1990) 16.
28. A. TODOROKI, H. KOBAYASHI AND K. MATUURA, *JSME Int. J. Series A Solid Mechanics Strength of Mater.* **38**(4) (1995) 524.
29 P. E. IRVING and C. THIAGARAJAN, *Smart Mater. Struct.* **7** (1998) 456.
30. X. WANG and D. D. L. CHUNG, *Polym. Compos.* **18**(6) (1997) 692.
31. *Idem. J. Mater. Res.* **14**(11) (1999) 4224.
32. S. WANG and D. D. L. CHUNG, *Polym. Compos.* **21**(1) (2000) 13.
33. D. A. GORDON, S. WANG and D. D. L. CHUNG, *Comp. Interf.* **11**(1) (2004) 95.
34. X. WANG and D. D. L. CHUNG, *Smart Mater. Struct.* **5** (1996) 796.

Received 3 January
and accepted 26 April 2005